Journal of Inorganic Biochemistry 196 (2019) 110693

Contents lists available at ScienceDirect

Journal of Inorganic Biochemistry

journal homepage: www.elsevier.com/locate/jinorgbio

Metal-dependent interactions of metallothionein-3 β-domain with amyloid-β peptide and related physiological implications

Zhongxiu Jiang[1], Baochai Shen[1], Juan Xiang*

College of Chemistry and Chemical Engineering, Central South University, Changsha 410083, PR China

ARTICLE INFO

Keywords:
Amyloid β peptide
Metallothionein-3 β-domain
Interaction
$Zn_3-\beta MT3/A\beta$ complex
Alzheimer's disease

ABSTRACT

Aberrant interactions of metal ions with amyloid-β peptide (Aβ) can potentiate Alzheimer's disease (AD) by participating in the aggregation process of Aβ and in the generation of reactive oxygen species (ROS). Metallothionein-3 (MT3), which is aberrantly expressed in AD brains, is believed to play an important role in the AD progression due to its ability of maintaining metal homeostasis and scavenging ROS. However, the related molecular mechanism is not clear. In this work, the metal-dependent interactions of MT3 β-domain (βMT3) with amyloid-β peptide (Aβ) were systematically studied. The results showed that $Zn_3-\beta MT3$ has a higher affinity to Aβ (K_d: ~0.7 μM) than $Cu_4-\beta MT3$ (K_d: ~22 μM). In $Zn_3-\beta MT3$, both Pro^7 and Pro^9 face outwards with their five-member rings in parallel, favoring their binding with aromatic residues via CH/π interactions. Two aromatic residues (Phe^4 and Tyr^{10}) in Aβ were identified as the specific binding sites for βMT3. Based on these, we posit a characteristic in-situ protection role of Zn-MT3 in inhibiting the Cu^{2+}-induced Aβ neurotoxicity, in which stable $Zn-MT3/A\beta$ complex forms via the $Zn_3-\beta MT3/A\beta$ interaction and effectively prevents the formation of $Cu-A\beta$ in high viscosity physiological fluids. Our results provide the mechanistic pathway and the specific roles of βMT3 in its protective bioactivity against AD progression, which means significant for elucidating the function of MT3 in AD neuropathology and for designing a MT3-related therapeutic strategy for AD.

1. Introduction

Alzheimer's disease (AD) is a progressive and devastating neurodegenerative pathology that affects several tens of millions of victims worldwide [1]. The morphological hallmarks of AD are extracellular amyloid plaques (or senile plaques), which are mainly constituted of amyloid β-peptide (Aβ) and transition metal ions (Zn^{2+} and Cu^{2+}) at high concentrations [2,3]. Cu^{2+} and Zn^{2+} are synaptically released and acts as a potent mediator of Aβ aggregation [4]. They can induce fast precipitation of Aβ, facilitate the oligomerization of Aβ and build up protease-resistant aggregates [5]. Compared with Zn^{2+}, Cu^{2+} has the additional property of producing strong extra-mitochondrial oxidative stress [6]. Also, Cu ions can activate protein kinase pathways, thereby increasing the secretion of matrix metalloproteinase, regulate the degradation of Aβ [7]. Given that aberrant interactions of metal ions Cu^{2+} with Aβ can potentiate AD, the endogenous molecules that uphold the metal homeostasis in the body appear to be a feasible therapeutic strategy. Metallothionein-3 (MT3), known as a regulator in the brain to maintain homeostasis of metal ions, has attracted attentions.

MT3 is one of four members of the mammalian MT family [8–10]. It is most prominently expressed in the central nervous system [11], enriched both in the intra- and extracellular space, and down-regulated in the AD brain [12]. Human MT3 contains 68 amino acids with 20 cysteine residues at the conserved positions [13,14]. Like other MT isoforms, metal-free MT3 (apo-MT3) binds Cu^{2+} and Zn^{2+} with high affinity, which enables its ability to regulate their transport and storage and inhibit their toxicity. In vitro, Zn–MT3 can alleviate the neurotoxic effects of Cu–Aβ (both soluble and aggregated) by suppressing the $Cu-A\beta$-mediated ROS production [15], in which the metal exchange between $Cu-A\beta$ and $Zn-MT3$ occurs via free Cu^{2+} has been suggested [16]. However, MT3 may play a more complicated role in AD progress. MT3, first identified as a neuronal growth-inhibitory factor, not only shares metal-binding and ROS-scavenging properties with other MTs, but also displays distinct protein-binding property not shared by other MT isoforms [10,14]. The protein-binding activity of MT3 arises from its β-domain (βMT3), while the α-domain is not directly involved [17,18]. The unique sequence to βMT3 is a TCPCP motif at positions 5–9 in the N terminus [8]. Apo-βMT3 is predominantly unstructured [30]. Once apo-βMT3 coordinates with Zn^{2+} or Cd^{2+}, the formation of a tightly bound metal-thiolate cluster yields a characteristic

* Corresponding author.
E-mail address: xiangj@csu.edu.cn (J. Xiang).
[1] Zhongxiu Jiang and Baochai Shen contributed equally to this work.

https://doi.org/10.1016/j.jinorgbio.2019.110693
Received 1 January 2019; Received in revised form 10 April 2019; Accepted 12 April 2019
Available online 13 April 2019
0162-0134/ © 2019 Elsevier Inc. All rights reserved.

conformational change of the TCPCP sequence, in which Pro^7 and Pro^9 residues are on the same side of the protein, both facing outward and the two 5-member rings of prolines are arranged almost in parallel, providing a potential interface for protein/protein interactions [19,20]. However, the coordination between Cu^{2+} and apo-βMT3 is quite different. Apo-βMT3 can efficiently reduce Cu^{2+} to Cu^{+} via concomitant disulfide formation and Cu^{+} binding [21], which must affect its protein-binding activity. Therefore, the affinity between βMT3 and Aβ, particularly the effects of metal ions on the βMT3/Aβ interactions, which mean significant for the elucidation of AD progress, need to be urgently elucidated.

In this work, the metal-dependent interactions of βMT3 with Aβ were studied by surface plasmon resonance (SPR). Apo-βMT3, Zn_3-βMT3 and Cu_4-βMT3 were investigated due to their potential correlation with the AD progress. The results showed that Zn_3-βMT3 has a higher affinity to Aβ (K_d: ~0.7 μM) than Cu_4-βMT3 (K_d: ~22 μM). With the usage of Aβ segments and the related mutations, two aromatic residues (Phe^4 and Tyr^{10}) in Aβ were identified as the specific binding sites for βMT3. Also, TCPCP motif at positions 5–9 in βMT3 was identified as the specific binding segment for Aβ. Due to the lack of TCPCP(5–9) sequence, MT2 has no specific affinity to Aβ. The affinities between Aβ and three βMT3 forms help us to understand the effect of βMT3 on preventing the Cu^{2+}-induced Aβ neurotoxicity, which means significant for elucidating the function of MT3 in AD neuropathology and for designing a MT3-related therapeutic strategy for AD.

2. Experimental section

2.1. Material and reagents

Lyophilized $Aβ_{1–42}$ was purchased from American Peptide Company (Sunnyvale, CA, USA). Lyophilized $Aβ_{1–16}$ and its mutants ($Aβ_{1–16}$(Y10A), $Aβ_{1–16}$(V12G), and $Aβ_{1–16}$(Y10A, V12G)), human apo-βMT3 and apo-βMT2, TCPCP pentapeptide were purchased from Shanghai Apeptide Co., Ltd. (Shanghai, China). Ethanolamine hydrochloride (AE), 11-Mercaptoundecanoic acid (MUA), N-hydroxysuccinimide (NHS), N-(3-Dimethylaminopropyl)-N′-ethylcarbodiimide hydrochloride (EDC), NaOH, NaH_2PO_4, Na_2HPO_4, 5,5′-dithio-bis-(2-nitrobenzoate) (DTNB), hexafluoroisopropanol (HFIP), and hydroxyethyl piperazine ethanesulfonic acid (HEPES) were acquired from Sigma (St. Louis, MO). All stock solutions were prepared daily with deionized water collected from a water purification system (Simplicity 185; Millipore, Milford, MA, USA).

2.2. Solution preparation

The $Aβ_{1–42}$ stock (0.5 mM) solutions were prepared according to the procedure conducted in our previous studies [22–24]. In brief, the purchased $Aβ_{1–42}$ was dissolved in HFIP at a final concentration of 1 $mg{\cdot}mL^{-1}$ and incubated overnight at 4 °C to dissolve any pre-existing oligomers. Then, the solution was sonicated for 30 min and lyophilized on freeze-dryer (Virtis Benchtop K, SP Scientific, Gardiner, NY). The lyophilized $Aβ_{1–42}$ was then dissolved in 10 mM NaOH solution. Upon sonication for 1 min, the solution was centrifuged at 13000 rpm for 30 min in an Eppendorf 5417R centrifuge (Eppendorf, Hamburg, Germany) to remove any insoluble particles, and the supernatants were pipetted out and diluted with HEPES (pH 7.4, 20 mM HEPES/100 mM NaCl) for the experiments. The concentration of the $Aβ_{1–42}$ monomer was calculated from the UV–vis spectra at 276 nm by setting the extinction coefficient ε of 1410 $M^{-1}{\cdot}cm^{-1}$ for tyrosine. All other Aβ stock solutions (200 μM) were prepared by directly dissolving the lyophilized samples in 10 mM NaOH at 4 °C. They were then diluted with HEPES to desired concentrations.

To avoid the oxidation of free thiol groups, all apo-βMT3-related solutions were prepared with nitrogen-saturated water and performed in a Mikrouna Ipure glove box (Mikrouna Co., Ltd., Shanghai, China) in which attainable O_2 concentration was below 1 ppm [25]. The apo-βMT3 stock solutions were prepared daily by dissolving 0.5 mM apo-βMT3 in 10 mM HEPES buffer. The concentration of apo-βMT3 solution was determined by assaying thiol groups with Ellman's reagent, DTNB [26]. Cu_4-βMT3 solution was prepared by incubating apo-βMT3 and Cu^{2+} at a molar ratio of 1:4 for 30 min. Zn_3-βMT3 solution was prepared by incubating apo-βMT3 and Zn^{2+} at a molar ratio of 1:3 for 30 min. The complete complexation of metal and apo-βMT3 in Cu_4-βMT3 and Zn_3-βMT3 solutions was confirmed by the disappearance of the characteristic absorption of free thiol groups at 412 nm with the addition of DTNB (Fig. S-1 in supporting information). The preparation processes of βMT2-related solutions (apo−βMT2, Cu_4-βMT2, and Zn_3-βMT2) were same as those of βMT3-related solutions. The Cu^{2+} and Zn^{2+} stock solution was separately prepared by dissolving 1 mM $CuCl_2$ or $ZnCl_2$ in 1 mM HCl solution.

2.3. Instruments

Flow-injection surface plasmon resonance measurements were conducted with a BI-SPR 3000 system equipped with BI-DirectFlow™ technology (Biosensing Instrument Inc., Tempe, AZ). The instrument can cut off the dispersed front and tail ends of injected sample plugs prior to introducing the samples into the SPR sensing areas. Kinetics data were fitted by Scrubber software (Biosensing Instrument Inc.) [22].

UV–visible spectra were carried out in quartz cuvettes (1 cm path lengths) on a UV-2450 spectrophotometer (Shimadzu, Kyoto, Japan). Dynamic-light-scattering measurements were conducted using a Zetasizer Nano ZS Instrument (Marlvern Instruments, Southborough, U.K.). Circular dichroism (CD) data were obtained with a Jasco-810 spectrophotometer (JASCO Corporation, Japan). Tyrosine fluorescence assays were performed on a FL-4600 Fluorescence Spectrophotometer (Hitachi High-Technology Co., Ltd., Tokyo, Japan). An excitation wavelength of 276 nm, emission at 315 nm, and an exit slit width of 10 nm were employed.

2.4. SPR measurements

The Au films coated onto BK7 glass slides were purchased from Biosensing Instrument Inc. (Tempe, AZ, USA) and were annealed in a hydrogen flame to eliminate surface contaminants. The MUA-covered SPR chip was formed by immersing the cleaned substrate in a 4.0 mM MUA ethanol solution for 12 h. Then, the chips were rinsed with ethanol and deionized water, and were dried with nitrogen for later use.

HEPES solution (pH 7.4, 20 mM HEPES/100 mM NaCl) was degassed via vacuum pumping for 30 min and was used as the carrier solution in all SPR measurements. The samples were preloaded into a 200 μL sample loop on a six-port valve and were then delivered to the flow cell with an internal volume of 1.0 μL with a syringe pump (Model KDS260, KD Scientific, Holliston, MA). In all SPR measurements, the flow rate was 100 μL/min. For on-line Aβ immobilization, after a stable baseline was obtained on the MUA chip, 200 μL aliquots of the EDC/NHS mixture (0.4 M EDC + 0.1 M NHS) were injected into the fluidic channel. Subsequently, with the injection of 200 μL aliquots of the Aβ solution, Aβ was immobilized onto the MUA chip via the standard amine coupling reaction. Finally, 1.0 M AE was injected to block the unreacted sites on the chip.

3. Results

3.1. Metal-dependent interactions of three βMT-3 forms with Aβ

The interactions of immobilized $Aβ_{1–42}$ with 10 μM apo-βMT3, Cu_4-βMT3, and Zn_3-βMT3 were determined by SPR, respectively. All three solutions induce corresponding SPR angle shifts (5.5 ± 0.2 mDeg

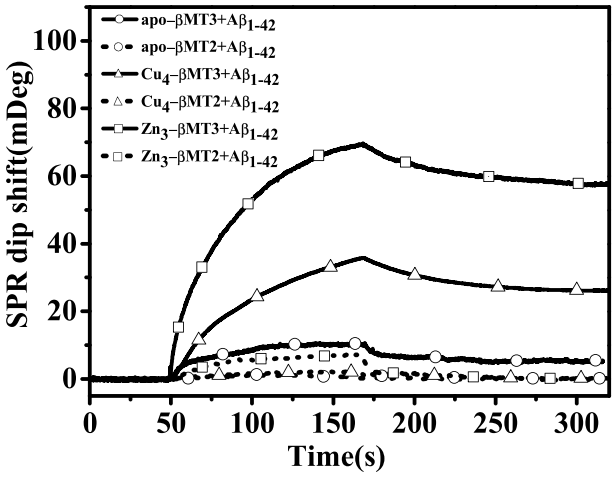

Fig. 1. The SPR responses from the injections of 10 μM apo-βMT3 (circular symbol curve), Cu_4-βMT3 (triangle symbol curve), and Zn_3-βMT3 (square symbol curve) onto the $Aβ_{1–42}$ modified Au flm surface, respectively. The dot curves correspond to the injection of 10 μM apo-βMT2 (circular symbol curve), Cu_4-βMT2 (triangle symbol curve), and Zn_3-βMT2 (square symbol curve), respectively.

for apo-βMT3, 26.0 ± 0.1 mDeg for Cu_4-βMT3, and 57.4 ± 0.2 mDeg for Zn_3-βMT3), as shown in Fig. 1. In contrast, the injection of apo-βMT2, Cu_4-βMT2, and Zn_3-βMT2 show no detectable SPR angle shifts, which confirms the characteristic affinity properties of three βMT3 forms with Aβ. The dissociation constants of different βMT3 forms binding to $Aβ_{1–42}$ were determined by simulating a series of binding curves obtained at different βMT3 concentrations (Fig. 2). After fitting these curves with the Scrubber program, the metal-dependent dissociation constant K_d were obtained for the $Aβ_{1–42}$/βMT3 interactions, as shown in Table 1. Zn_3-βMT3 displays a much stronger affinity to Aβ (K_d: ~0.7 μM) than Cu_4-βMT3 (K_d: ~22 μM) and apo-βMT3 (K_d: ~19 μM).

3.2. Binding sites of βMT-3 interacting with $Aβ_{1–42}$

To reveal the effect of βMT3 on the Aβ-related neurotoxicity, the binding chemistry of Aβ interacting with βMT3 was thoroughly explored. Here, two typical truncated Aβ forms, hydrophilic $Aβ_{1–16}$ and hydrophobic $Aβ_{12–28}$, which are respectively related with the peptide's properties of metal coordination and peptide aggregation, were used to judge the interaction region of Aβ with βMT3. Fig. 3 displays that the independent injections of apo-βMT3, Cu_4-βMT3, and Zn_3-βMT3 onto

Table 1
K_d of $Aβ_{1–16}$ and $Aβ_{1–42}$ to apo-βMT3, Zn_3-βMT3 and Cu_4-βMT3.

	K_d (μM)			
	$Aβ_{1–42}$	$Aβ_{1–16}$	$Aβ_{1–16}$(F4A)	$Aβ_{1–16}$(Y10A)
apo-βMT3	19 ± 3	14 ± 10	88 ± 60	72 ± 30
Zn_3-βMT3	0.7 ± 0.3	0.2 ± 0.2	83 ± 50	77 ± 70
Cu_4-βMT3	22 ± 10	17 ± 10	70 ± 70	83 ± 70

the $Aβ_{1–16}$ modified surface induce the corresponding concentration-dependent SPR angle shifts, respectively. In contrast, only slight SPR angle shift (< 1 mDeg) from nonspecific adsorption was observed on the $Aβ_{12–28}$ modified surface (Fig. S-2 in supporting information). In this event, it can be concluded that all three βMT3 forms interact with the hydrophilic domain of Aβ. After fitting these curves with the Scrubber program, the similar trend in the metal-dependent dissociation constant K_d were obtained on the immobilized $Aβ_{1–16}$ surface (Table 1), which confirms further that the Aβ/βMT3 interactions mainly involves the hydrophilic domain of $Aβ_{1–42}$.

Fig. 4 displays the tyrosine fluorescence of $Aβ_{1–16}$ after addition of Zn_3-βMT3 or Cu_4-βMT3 at different molar ratios. The significant intensity changes indicate the aromatic group amino acids in $Aβ_{1–16}$ as the possible binding site on the MT3/Aβ interactions. Thus, the roles of Phe^4 and Tyr^{10}, two typical aromatic group amino acids in $Aβ_{1–16}$, were investigated. SPR detections were performed with the independent injection three $Aβ_{1–16}$ solutions whose Tyr or Phe residue was mutated with Ala ($Aβ_{1–16}$(Y10A), $Aβ_{1–16}$(F4A), and $Aβ_{1–16}$(F4A, Y10A)). Zeta potential and CD measurements show no discernible changes in the surface charge and structure of the mutants (Fig. S-3 in supporting information), confirming the viability of the mutants for binding studies. Fig. 5A reveals that the injection of apo-βMT3 onto a single site mutation produces small SPR angle shifts (3.5 ± 0.2 mDeg for $Aβ_{1–16}$(Y10A) and 7.5 ± 0.2 mDeg for $Aβ_{1–16}$(F4A)). It is quite different from the results of $Aβ_{1–16}$ modified surface, which has an angle shift of ~15.0 mDeg. Also, the dissociation constant of apo-βMT3 with $Aβ_{1–16}$(Y10A) and $Aβ_{1–16}$(F4A) were obtained with the Scrubber program, respectively. As shown in Table 1, both K_d values are nearly five times larger than those from $Aβ_{1–16}$. Furthermore, the injection of apo-βMT3 onto $Aβ_{1–16}$(F4A, Y10A) induces no detectable SPR angle shift. This instance indicates no specific interactions between apo-βMT3 and $Aβ_{1–16}$(F4A, Y10A). Therefore, both Phe^4 and Tyr^{10} should be the candidate of the predominant binding site for the interaction of $Aβ_{1–16}$ with apo-βMT3. Similar Aβ binding features were observed for Zn_3-βMT3 and Cu_4-βMT3 (Fig. 5B and C). It indicates that despite the different affinities, three βMT3 forms bind onto Aβ at the same sites, the Phe^4 and Tyr^{10}.

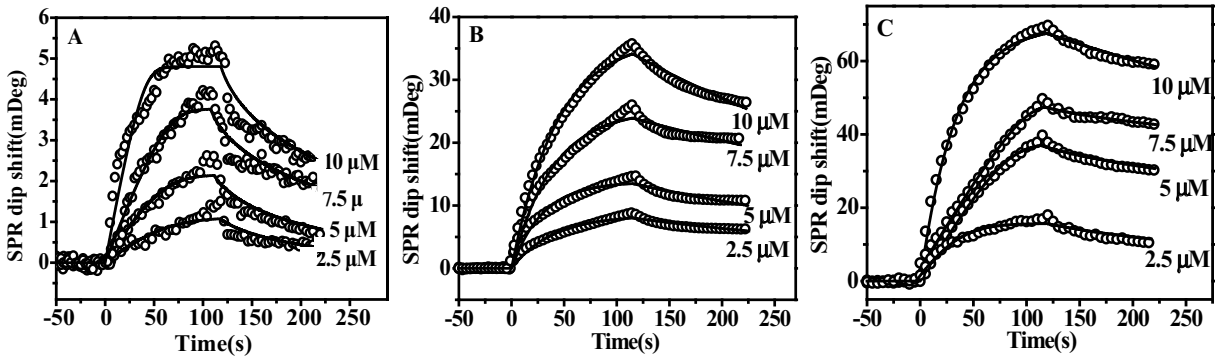

Fig. 2. Non-linear fitting curves of the immobilized $Aβ_{1–42}$ bound to apo-βMT3 (A), Cu_4-βMT3 (B), and Zn_3-βMT3 (C) under different concentrations at pH 7.4, obtained by the Scrubber program. The corresponding experimental data were obtained at and shown as hollow circular symbols.

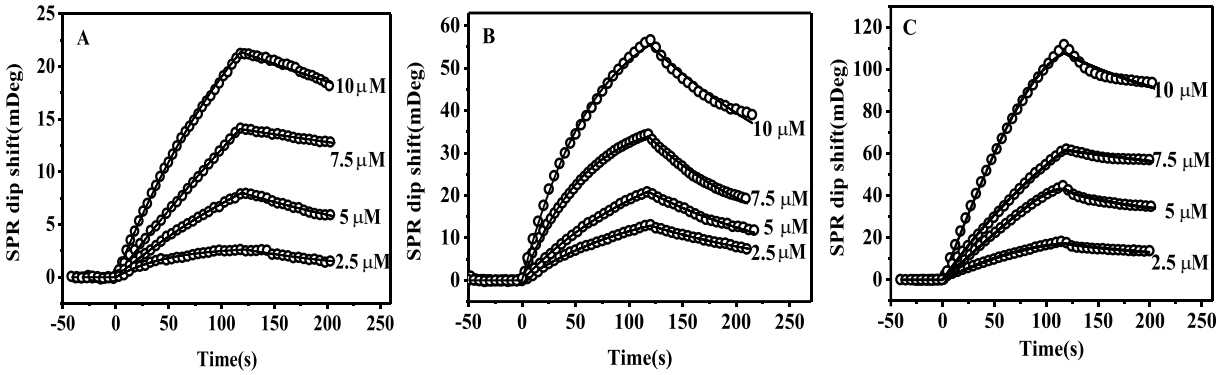

Fig. 3. Non-linear fitting curves of the immobilized $A\beta_{1-16}$ bound to apo-βMT3 (A), Cu_4-βMT3 (B), and Zn_3-βMT3 (C) under different concentrations at pH 7.4, obtained by the Scrubber program. The corresponding experimental data are shown as hollow circular symbols.

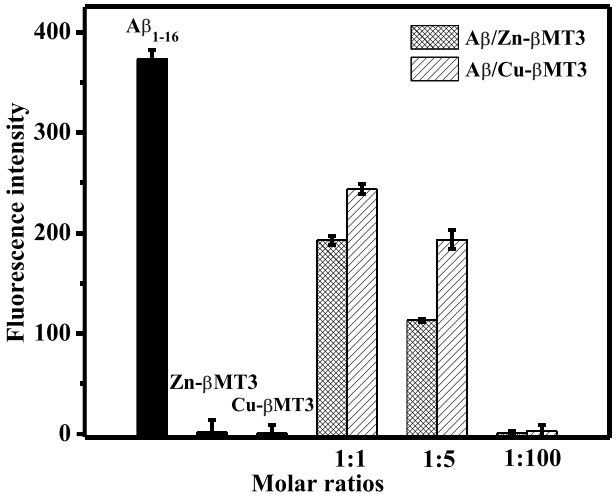

Fig. 4. Tyrosine fluorescence of 10 μM $A\beta_{1-16}$ after addition of Zn_3-βMT3 or Cu_4-βMT3 at different molar ratios.

The binding sites of βMT3 for the βMT3/Aβ interactions were also explored. Fig. 1 has demonstrated that all three βMT3 forms are capable of binding Aβ but the corresponding βMT2 forms are unable. The great difference should be attributed to the distinct sequence of βMT3, a threonine at position 5 and a conserved CPCP(6–9) motif which are absent in βMT2. To verify the deduction, the SPR responses with the injection of TCPCP pentapeptide on the immobilized $A\beta_{1-16}$ were performed. As shown in Fig. 6, TCPCP concentration-dependent SPR angle shifts appear, confirming the specific interaction between $A\beta_{1-16}$ and TCPCP. After fitting these curves with the Scrubber program, the dissociation constant K_d of $A\beta_{1-16}$/TCPCP was obtained as 21 μM. Obviously, compared with $A\beta_{1-16}$/TCPCP, $A\beta_{1-16}/Zn_3-$βMT3 has a much stronger affinity. It can be attributed to the characteristic conformation of the TCPCP(5–9) sequence in the Zn_3-βMT3, where both Pro^7 and Pro^9 face outwards with their five-member rings arranged almost in parallel, while Thr^5 is at the opposite side of the two rings. This characteristic conformation around the TCPCP(5–9) sequence in Zn-MT3 has been suggested to provide an interacting interface for protein-protein interactions [27,28]. Due to the reduction of Cu^{2+} to Cu^+ and the formation of cysteine disulfide [29], Cu_4-βMT3 display different conformation from Zn_3-βMT3, which should be responsible for its weak affinity to Aβ. In the absence of metals, apo-MT3 is predominantly unstructured [30], which induces its weak affinity to Aβ.

4. Discussion

Our studies revealed the metal-dependent interactions between βMT3 and Aβ. By use some mutants, we confirmed the specific binding sites of Pro^7 and Pro^9 in three βMT3 forms and Phe^4 and Tyr^{10} in Aβ. The dissociation constants from single-point mutated Aβ ($A\beta_{1-16}$(Y10A) and $A\beta_{1-16}$(F4A)) are at ~100 μM, which is accordant with the affinity of CH/π interactions [31]. In Zn_3-βMT3, both Pro^7 and Pro^9 face outwards with their five-member rings in parallel, favoring their binding with aromatic residues via CH/π interactions. As a result, Zn_3-βMT3 displays a higher affinity to Aβ (K_d: ~0.7 μM) than Cu_4-βMT3 (K_d: ~22 μM).

In the brain, MT3 is found both in the intracellular and extracellular space where its concentration is at μM grade [32]. It means only the Aβ/Zn−MT3 complex via the $A\beta/Zn_3-$βMT3 interaction is stable in vivo. Based on it, the protection effect of Zn−MT3 from Cu^{2+}-induced Aβ neurotoxicity can be deduced. As depicted in Fig. 7, aberrant interactions between Cu^{2+} and Aβ can potentiate AD by inducing the formation of neurotoxic Aβ aggregates (Aβ oligomer, protofibrils, and fibrils) [33] as well as promoting the generation of ROS by the redox cycling of Cu−Aβ complexes [34,35]. Because of its high redox activity, Cu^{2+} can interact with Aβ, catalyzing the generation of H_2O_2 through a reduction process that uses O_2 and bioavailable reducing agents such as vitamin C (VC), cholesterol, and catecholamines (Fig. 7A). In the absence of sufficient detoxifying enzymes, H_2O_2 can lead to a further generation of hydroxyl radicals through the Fenton reaction with relevant consequent neurotoxic effects, producing strong extra-mitochondrial oxidative stress. However, with the presence of Zn−MT3, stable Aβ/Zn−MT3 complex is formed via the $A\beta/Zn_3-$βMT3 interaction. Once free or weak coordinated Cu^{2+} close to the complex, due to the higher affinity of MT3 to Cu^{2+} than to Zn^{2+} ($\sim10^{-11}$ M) [36,37], Zn-MT3 must capture Cu^{2+}. Meanwhile, the released Zn^{2+} is transferred into Aβ due to the affinity between Aβ and Zn^{2+} (10^{-4}–10^{-7} M) [13–16]. With the formation of Cu−MT3 and Zn−Aβ, the weakened affinity induces the dissociation of the Aβ/MT3 complex (Fig. 7B). This deduction was confirmed in vitro by a tyrosine fluorescence experiment (Fig. S-4 in supporting information). After adding Zn_3–βMT3 into Cu–Aβ solution, the obtained fluorescence intensity was close to the Zn–Aβ solution. It confirmed the metal exchange between Zn_3–βMT3 and Cu–Aβ, and the formation of Zn–Aβ.

The whole metal-exchange and dissociation process is anticipated to greatly reduce the neurotoxicity in vivo. First, the Cu−Aβ complex is replaced with Zn−Aβ. Due to the redox silence of Zn^{2+} [38], the ROS production is less. In addition, Zn^{2+} binding is associated with the formation of more amorphous Aβ aggregates that is less neurotoxic [39]. Second, the dissociation of the Aβ/MT3 complex favors the

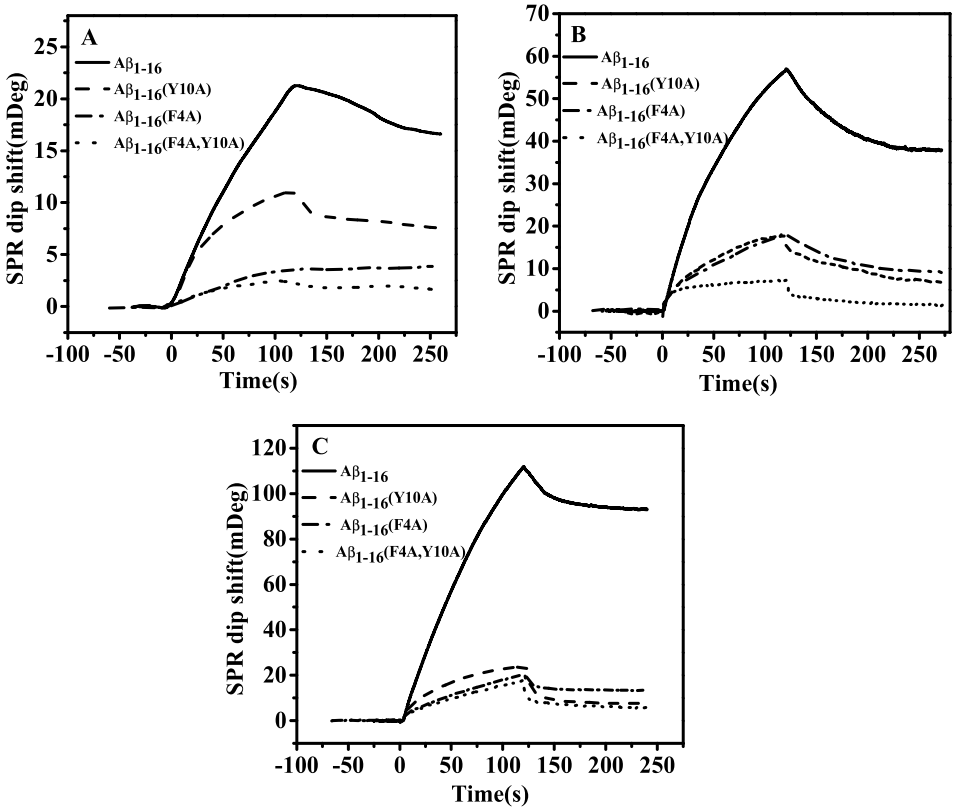

Fig. 5. The SPR responses from the injection of 10 μM apo-βMT3 (panel A) onto the Au film modified with $A\beta_{1-16}$ or its mutants, respectively. Panel B and C corresponds to the injection of $Cu_4-\beta MT3$ and $Zn_3-\beta MT3$, respectively.

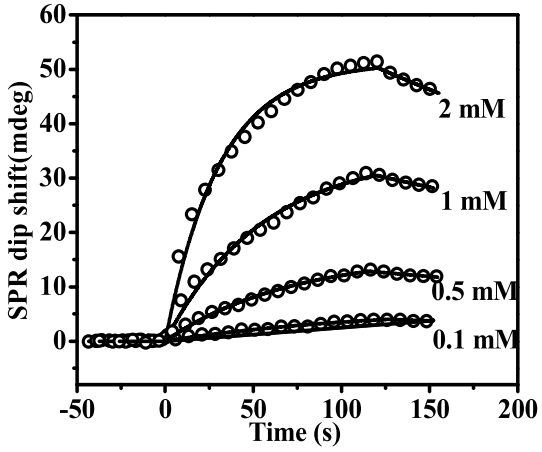

Fig. 6. Non-linear fitting curves of the immobilized $A\beta_{1-16}$ bound to TCPCP pentapeptide under different concentrations at pH 7.4, obtained by the Scrubber program. The corresponding experimental data are shown as hollow circular symbols.

clearance of Cu−MT3. MT3 is one of the most important species for Cu^{2+} homeostasis in the brain. Once overexpressed Cu^{2+} is captured by MT3, the degradation of Cu−MT3 is processed mainly by the lysosomal protease such as cathepsin B [40]. The dissociation of the Aβ/MT3 complex is necessary for the structural recognition between the protease and Cu−MT3.

Cu^{2+} interacts with Aβ and induces its aggregation within a rapid timeframe [41]. Therefore, the formation of Cu−Aβ complex is the key step in Cu^{2+}-induced Aβ neurotoxicity. With the formation of Zn−MT3/Aβ complex, Zn−MT3 can effectively prevent the formation of Cu−Aβ complex via the in-situ capture of free or weak coordinated Cu^{2+}. Zn−MT2 can also decrease Cu^{2+}-induced Aβ neurotoxicity [42]. Due to the lack of TCPCP(5–9) sequence, Zn−MT2 has no specific affinity to Aβ. Therefore, Zn−MT2 usually performs ex-situ protection via the capture of Cu^{2+} from the Cu−Aβ complex. In vitro studies usually perform in PBS or HEPES buffer which has low viscosity (~1 cP). Due to the quickly molecular motions, Zn−MT2 can quickly capture Cu^{2+} from the Cu−Aβ complex. Therefore, the in-situ and ex-situ protection may display no significant difference. However, in physiological condition, both intracellular and intercellular fluids have much higher viscosity (above 1.85 cP) in which the molecular motions slow down [43]. As a result, the Cu−Aβ complex cannot be quickly cleansed by Zn−MT2, which may induce the neurotoxicity. Only the in-situ protection of MT3 can effectively prevent the formation of Cu−Aβ complex. In this regard, MT3 plays a more efficient protection against Aβ neurotoxicity in AD.

5. Conclusion

In this work, we systematically studied the metal-dependent interactions between βMT3 and Aβ. The results showed that $Zn_3-\beta MT3$ has a higher affinity to Aβ than $Cu_4-\beta MT3$. In $Zn_3-\beta MT3$, both Pro^7 and Pro^9 face outwards with their five-member rings in parallel, favoring their binding with aromatic residues via CH/π interactions. Two aromatic residues (Phe^4 and Tyr^{10}) in Aβ were identified as the specific binding sites for MT3. Due to the concentration of MT3 in vivo (~1 μM), only the Zn−MT3/Aβ complex via the $A\beta/Zn_3-\beta MT3$ interaction is stable in the real systems. Based on it, we posited a characteristic protection role of Zn−MT3 in inhibiting the Cu^{2+}-induced Aβ neurotoxicity. In which, Zn−MT3/Aβ complex forms under physiological conditions, preventing the formation of Cu−Aβ via the in-situ capture of free or weak coordinated Cu^{2+}. Our results provide the mechanistic pathway and the specific roles of MT3 in its protective bioactivity against AD progression, which is significant for

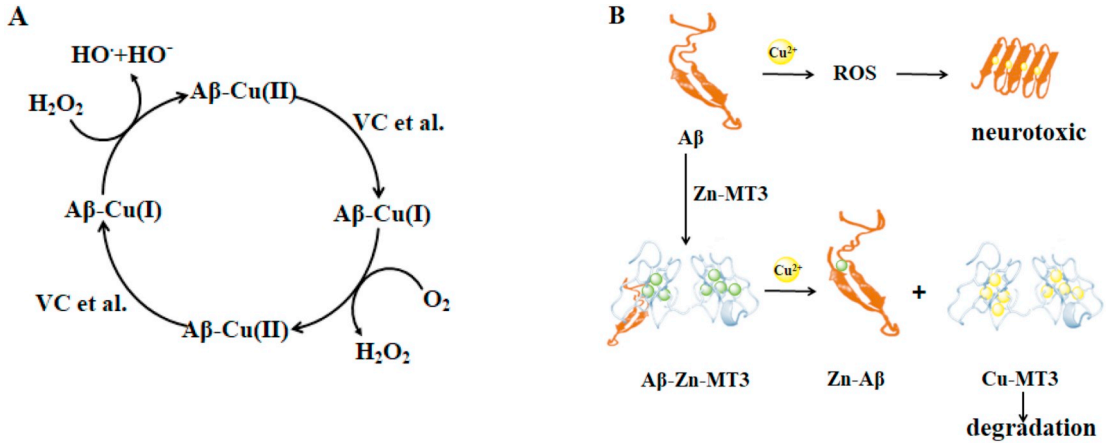

Fig. 7. Reaction scheme of the redox cycling of Cu − Aβ complexes (A) and the possible protection of MT3 from Cu^{2+}-induced Aβ neurotoxicity (B).

understanding the function of MT3 in AD neuropathology and for designing a MT3-related therapeutic strategy for AD.

Abbreviations

AD	Alzheimer's disease
Aβ	amyloid-β peptide
apo-βMT3	Human metal-free βMT3
apo-βMT2	Δ5–9 mutant
ROS	reactive oxygen species
MT3	Metallothionein-3
βMT3	MT3 β-domain
SPR	surface plasmon resonance
AE	Ethanolamine hydrochloride
MUA	11-Mercaptoundecanoic acid
NHS	N-hydroxysuccinimide
EDC	N-(3-Dimethylaminopropyl)-N′-ethylcarbodiimide hydrochloride
DTNB	5,5′-dithio-bis-(2-nitrobenzoate)
HFIP	hexafluoroisopropanol
HEPES	hydroxyethyl piperazine ethanesulfonic acid
VC	vitamin C

Acknowledgment

This work was supported by the National Natural Science Foundation of China (21573290, 21273288).

Appendix A. Supplementary data

Supplementary data to this article can be found online at https://doi.org/10.1016/j.jinorgbio.2019.110693.

References

[1] Alzheimer's Association, Alzheimer's association report: 2014 Alzheimer's disease facts and figures, Alzheimers Dement. 10 (2014) 47–92.
[2] C.L. Masters, G. Simms, N.A. Weinman, G. Multhaup, B.L. McDonald, K. Beyreuther, Amyloid plaque core protein in Alzheimer disease and down syndrome, Proc. Natl. Acad. Sci. U. S. A. 82 (1985) 4245–4249.
[3] M.A. Lovell, J.D. Robertson, W.J. Teesdale, J.L. Campbell, W.R. Markesbery, Copper, iron and zinc in Alzheimer's disease senile plaques, J. Neurol. Sci. 158 (1998) 47–52.
[4] P. Zatta, D. Drago, S. Bolognin, S.L. Sensi, Alzheimer's disease, metal ions and metal homeostatic therapy, Trends Pharmacol. Sci. 30 (2009) 346–355.
[5] A.I. Bush, The metallobiology of Alzheimer's disease, Trends Neurosci. 26 (2003) 207–214.
[6] V. Frazzini, E. Rockabrand, E. Mocchegiani, S.L. Sensi, Oxidative stress and brain aging: is zinc the link? Biogerontology 7 (2006) 307–314.
[7] K.J. Yin, J.R. Cirrito, P. Yan, X. Hu, Q. Xiao, X. Pan, R. Bateman, H. Song, F.F. Hsu, J. Turk, J. Xu, C.Y. Hsu, J.C. Mills, D.M. Holtzman, J.M. Lee, Matrix metalloproteinases expressed by astrocytes mediate extracellular amyloid-beta peptide catabolism, J. Neurosci. 26 (2006) 10939–10948.
[8] Z.C. Ding, F.Y. Ni, Z.X. Huang, Neuronal growth-inhibitory factor (metallothioneein-3): structure-function relationships, FEBS J. 277 (2010) 2912–2920.
[9] P. Faller, Neuronal growth-inhibitory factor (metallothionein-3): reactivity and structure of metal-thiolate clusters, FEBS J. 277 (2010) 2921–2930.
[10] C. Hwells, A.K. West, R.S. Chung, Neuronal growth-inhibitory factor (metallothionein-3): evaluation of the biological function of growth-inhibitory factor in the injured and neurodegenerative brain, FEBS J. 277 (2010) 2931–2939.
[11] P.A. Binz, J.H.R. Kagi, Metallothionein: Molecular evolution and classification, Metallothionein IV, 1999.
[12] W. Xu, Q.M. Xu, H. Cheng, X.S. Tan, The efficacy and pharmacological mechanism of Zn_7-MT3 to protect against Alzheimer's disease, Sci. Rep. 7 (2017) 13763.
[13] R.D. Palmiter, S.D. Findley, T.E. Whitmore, D.M. Durnam, MT-3, a brain-specific member of the metallothionein gene family, Proc. Natl. Acad. Sci. U. S. A. 89 (1992) 6333–6337.
[14] Y. Uchida, K. Takio, K. Titani, Y. Ihara, M. Tomonaga, The growth inhibitory factor that is deficient in the Alzheimer's disease brain is a 68 amino acid metallothionein-like protein, Neuron 7 (1991) 337–347.
[15] G. Meloni, V. Sonois, T. Delaine, L. Guilloreau, A. Gillet, J. Teissie, P. Faller, M. Vašák, Metal swap between Zn-7-metallothionein-3 and amyloid-beta-Cu protects against amyloid-beta toxicity, Nat. Chem. Biol. 4 (2008) 366–372.
[16] J.T. Pedersen, C. Hureau, L. Hemmingsen, N.H.H. Heegaard, G. Ostergaarg, M. Vašák, P. Faller, Rapid metal between Zn-7-metallothionein-3 amyloid-beta peptide promotes amyloid-related structural changes, Biochemistry 51 (2012) 1697–1706.
[17] Y. Uchida, Y. Ihara, The N-terminal portion of growth inhibitory factor is sufficient for biological activity, J. Biol. Chem. 270 (1995) 3365–3369.
[18] A.K. Sewell, L.T. Jensen, J.C. Erickson, R.D. Palmiter, D.R. Winge, Bioactivity of metallothionein-3 correlates with its novel beta domain sequence rather than metal binding properties, Biochemistry 34 (1995) 4740–4747.
[19] F.Y. Ni, B. Cai, Z.C. Ding, F. Zheng, M.J. Zhang, H.M. Wu, H.Z. Sun, Z.X. Huang, Structural prediction of the β-domain of metallothionein-3 by molecular dynamics simulation, Proteins 68 (2007) 255–266.
[20] M.P. Williamson, The structure and function of proline-rich regions in proteins, Biochem. J. 297 (1994) 249–260.
[21] E. Artells, O. Palacios, M. Capdevila, S. Atrian, In vivo-folded metal-metallothionein 3 complexes reveal the Cu-thionein rather than Zn-thionein character of this brain-specific mammalian metallothionein, FEBS J. 281 (2014) 1659–1678.
[22] M.M. Liu, L. Kou, Y.N. Bin, L.P. Wan, J. Xiang, Complicated function of dopamine in Aβ-related neurotoxicity: dual interactions with Tyr^{10} and SNK (26–28) of Aβ, J. Inorg. Biochem. 164 (2016) 119–128.
[23] C. Deng, H. Liu, M. Zhang, H. Deng, C. Lei, L. Shen, B. Jiao, Q. Tu, Y. Jin, L. Xiang, W. Deng, Y. Xie, J. Xiang, A light-up non-thiolated aptasensor for low-mass soluble amyloid-β_{40} oligomers at high salt concentrations, Anal. Chem. 90 (2018) 1710–1717.
[24] C.Y. Deng, M.M. Zhang, C.Y. Liu, H.H. Deng, Y. Huang, M.H. Yang, J. Xiang, B. Ren, Electrostatic force triggering elastic condensation of double-stranded DNA for high-performance one-step immunoassay, Anal. Chem. 90 (2018) 11446–11452.
[25] M. Zhang, Q.Y. Zhai, L.P. Wan, L. Chen, Y. Peng, C.Y. Deng, J. Xiang, J.W. Yan, Electrochemical impedance spectroscopy for real-time detection of lipid membrane damage based on a porous self-assembly monolayer support, Anal. Chem. 90 (2018) 7422–7427.
[26] P.J. Sadler, H.Y. Li, H.Z. Sun, Coordination chemistry of metals in medicine: target sites for bismuth, Coord. Chem. Rev. 185-186 (1999) 689–709.
[27] F. Ni, B. Cai, Z. Ding, F. Zheng, M. Zhang, H. Wu, H. Sun, Z. Huang, Structural prediction of the beta-domain of metallothionein-3 by molecular dynamics simulation, Proteins 68 (2010) 255–266.
[28] H. Yu, J.K. Chen, S. Feng, D.C. Dalgarno, A.W. Brauer, S.L. Schreiber, Structural basis for the binding of proline-rich peptides to SH3 domains, Cell 76 (1994) 933–945.

[29] G. Meloni, P. Faller, M. Vašák, Redox silencing of copper in metal-linked neurodegenerative disorders: reaction of Zn-7-metallothionein-3 with Cu^{2+} ions, J. Biol. Chem. 282 (2007) 16068–16078.
[30] N. Romero-Isart, L.T. Jensen, O. Zerbe, D.R. Winge, M. Vašák, Engineering of metallothionein-3 neuroinhibitory activity into the inactive isoform metallothionein-1, J. Biol. Chem. 277 (2002) 37023–37028.
[31] R.U. Kadam, D. Garg, J. Schwartz, R. Visini, M. Sattler, A. Stocker, T. Darbre, J.L. Reymond, CH-π "T-shape" interaction with histidine explains binding of aromatic galactosides to pseudomonas aeruginosa lectin LecA, ACS Chem. Biol. 8 (2013) 1925–1930.
[32] M.A.M. Rodrigo, S. Dostalova, H. Buchtelova, V. Strmiska, P. Michalek, S. Krizkova, A. Vicha, P. Jencova, T. Eckschlager, M. Stiborova, Z. Heger, V. Adam, Comparative gene expression profiling of human metallothionein-3 up-regulation in neuroblastoma cells and its impact on susceptibility to cisplatin, Oncotarget 9 (2018) 4427–4439.
[33] S. Jun, S. Saxena, The aggregated state of amyloid-β peptide in vitro depends on Cu^{2+} ion concentration, Angew. Chem. Int. Ed. 46 (2007) 3959–3961.
[34] X. Huang, C.S. Atwood, M.A. Hartshorn, G. Multhaup, L.E. Goldstein, R.C. Scarpa, M.P. Cuajungco, D.N. Gray, J. Lim, R.D. Moir, R.E. Tanzi, A.I. Bush, The Aβ peptide of Alzheimer's disease directly produces hydrogen peroxide through metal ion reduction, Biochemistry 38 (1999) 7609–7616.
[35] V. Balland, C. Hureau, J.M. Saveant, Electro-chemical and homogeneous electron transfers to the Alzheimer amyloid-β copper complex follow a preorganization mechanism, Proc. Natl. Acad. Sci. U. S. A. 107 (2010) 17113–17118.
[36] D.H. Hamer, Metallothionein, Annu. Rev. Biochem. 55 (1985) 913–951.
[37] D.W. Hasler, L.T. Jensen, O. Zerbe, D.R. Winge, M. Vašák, Effect of the two conserved prolines of human growth inhibitory factor (metallothionein-3) on its biological activity and structure fluctuation: comparison with a mutant protein, Biochemistry 39 (2010) 14567–14575.
[38] M.P. Cuajungco, L.E. Goldstein, A. Nunomura, M.A. Smith, J.T. Lim, C.S. Atwood, X. Huang, Y.W. Farrag, G. Perry, A.I. Bush, Evidence that the β-amyloid plaques of Alzheimer's disease represent the redox-silencing and entombment of Aβ by zinc, J. Biol. Chem. 275 (2000) 19439–19442.
[39] K. Garai, B. Sahoo, S.K. Kaushalya, R. Desai, S. Maiti, Zinc lowers amyloid-β toxicity by selectively precipitating aggregation intermediates, Biochemistry 46 (2007) 10655–10663.
[40] K.S. Min, T. Nakatsubo, Y. Fujita, S. Onosaka, K. Tanaka, Degradation of cadmium metallothionein in vitro by lysosomal proteases, Toxicol. Appl. Pharmacol. 113 (1992) 299–305.
[41] J.T. Pedersen, C.B. Borg, T.C. Michaels, T.P. Knowles, P. Faller, K. Teilum, L. Hemmingsen, Aggregation-prone amyloid-β-Cu^{2+} species formed on the millisecond timescale under mildly acidic conditions, ChemBioChem 16 (2015) 1293–1297.
[42] R.S. Chung, C. Howells, E.D. Eaton, L. Shabala, K. Zovo, P. Palumaa, R. Sillard, A. Woodhouse, W.R. Bennett, S. Ray, J.C. Vickers, A.K. West, The native copper- and zinc-binding protein metallothionein blocks copper-mediated Aβ aggregation and toxicity in rat cortical neurons, PLoS One 5 (2010) 12030.
[43] I.C. Cowan, J. Harkness, The plasma viscosity in rheumatic diseases, Brit. Med. J. 2 (1947) 686–688.